IEEE Access
Multidisciplinary | Rapid Review | Open Access Journal

Received 5 July 2024, accepted 25 July 2024, date of publication 30 July 2024, date of current version 7 August 2024.

Digital Object Identifier 10.1109/ACCESS.2024.3435694

RESEARCH ARTICLE

Remaining Useful Life Prediction for Pressurized Fluid Pipelines Based on Acoustic Emission Monitoring and an Adaptive Fuzzy Similarity Measure

DUC-THUAN NGUYEN[1], TUAN-KHAI NGUYEN[1], ZAHOOR AHMAD[1], AND JONG-MYON KIM[1,2]

[1]Department of Electrical, Electronic and Computer Engineering, University of Ulsan, Ulsan 44610, South Korea
[2]Prognosis and Diagnostics Technologies Company Ltd., Ulsan 44610, South Korea

Corresponding author: Jong-Myon Kim (jmkim07@ulsan.ac.kr)

This work was supported in part by Ulsan City & Electronics and Telecommunications Research Institute (ETRI) funded by Ulsan City through the Development of Intelligentization Technology for the Main Industry for Manufacturing Innovation and Human-Mobile-Space Autonomous Collaboration Intelligence Technology Development in Industrial Sites under Grant 24AB1600, and in part by Korea Institute of Energy Technology Evaluation and Planning (KETEP) funded by Korean Government [Minister of Trade, Industry and Energy (MOTIE)] through the Development of Life Prediction Safety Technology and Hydrogen Embrittlement Estimation of Liquefied Natural Gas (LNG) Pipe Mixed Hydrogen under Grant RS-2023-00232515.

ABSTRACT Pressurized fluid pipelines are among the most crucial components in industrial settings. Operating under high pressure leads to pipeline susceptibility to cracking, rupture, and significant damage. Monitoring the condition and predicting the remaining useful life before the failure of pressurized pipes are essential for informed and timely maintenance decisions. In this work, we propose a novel method for predicting the remaining useful life of pressurized pipelines based on acoustic emission monitoring and similarity-based learning. Specifically, acoustic emission sensors are deployed to record acoustic emission events caused by cracks in the pipeline. A pipeline health indicator is proposed based on accumulated events detected through a constant false alarm rate signal detector. Leveraging the historical run-to-fail trajectories of the health indicator, a similarity measure is introduced to predict the remaining pipeline life. This method computes the similarity between the current health indicator trajectory and past trajectories based on a Euclidean distance in the proposed derivative convolutional domain. Trajectory similarity determines the remaining lifetime similarity, which is weighted using data-adaptive fuzzy rules to estimate the current remaining useful life. Elaborate experimental validations are conducted on a custom pressurized pipeline system in a laboratory setting. Experimental results demonstrate the high efficacy of the proposed method in predicting the remaining useful life of the pipeline, surpassing other commonly used methods in both accuracy and certainty.

INDEX TERMS Remaining useful life, pipelines, acoustic emission, fuzzy logic, similarity learning.

I. INTRODUCTION

Fluid pipeline systems are indispensable components in industrial settings [1]. Their primary function is to transport various substances such as gasoline, diesel, natural gas, water, and steam [2], [3], [4], [5]. Moreover, pipelines are used for transporting compressed air and chemicals in industrial processes [6], [7]. Their widespread use is attributed to their cost-effectiveness, safety, and capability to transport large volumes of fluids [8]. However, pipelines are susceptible to detrimental factors leading to deterioration, such as corrosion, cracking, and rupture after prolonged use [9]. These pose hazards of severe consequences like resource loss, environmental pollution, and substantial economic damage [10].

The associate editor coordinating the review of this manuscript and approving it for publication was Xiao-Sheng Si.

Particularly, in industrial processes such as chemical production and nuclear power, pipelines under high pressure (pressurized pipelines) frequently encounter higher risks of destruction, posing numerous dangers [11], [12], [13], [14]. Therefore, monitoring the condition of pressurized pipelines is a mandatory requirement in production activities to ensure their safety, stability, and reliability. Furthermore, pressurized pipelines often operate under specific known profiles, involving pre-set changes in flow rates and pressures [15], [16]. This provides the potential for forecasting health conditions, such as the remaining useful life (RUL), of pressurized pipelines. Based on the preliminary analyses of necessity and feasibility, this study focuses on developing methods for monitoring the health condition and predicting the RUL of pressurized pipelines in industrial processes.

Generally, monitoring of pressurized pipelines can be conducted through various methods, such as pressure and flow rate monitoring [17], acoustic emission (AE) monitoring [18], [19], or visual inspection [20]. For such pipelines, it is crucial to track and to predict their condition before failure, specifically concerning cracks and ruptures [21]. While monitoring flow rate and pressure promptly can detect ruptures in pipelines due to immediate fluctuation, it is challenging to predict precursor symptoms, such as cracks, of malfunction [22]. Visual inspection might better identify early signs of damage by assessing pipe surface conditions, such as deformities. However, this typically requires human labor and faces major limitations in accessing buried pipelines, those in difficult-to-reach areas, or detecting damages within the inner layers of a pipeline [23].

AE monitoring is considered the most promising monitoring method for such pipes because it can predict events due to high sensitivity to discontinuities along the pipe [24]. Even a small discontinuity, such as a small crack, can be detected by AE sensors, a feat that cannot be accomplished through other methods [10], [25]. Moreover, AE sensors can continuously monitor equipment and pipelines in real time, enabling the tracking of pipeline degradation [26]. Recently, Quy et al. [27] presented a novel method for detecting and localizing cracks in a high-pressure fluid pipeline using AE signals by scanning peaks in signal channels in the time-frequency domain. These peaks were filtered to determine genuine AE events, and the time difference of arrival technique was used to localize the position of the leak. Livadiotis et al. [28] introduced a new approach to consider the helical propagation of AE events caused by helical guided waves (HGW) for monitoring corrosion in steel pipelines. Using the amplitudes of these events, a qualitative corrosion monitoring approach employing b-value analysis was proposed. Huang et al. [29] proposed a lightweight neural network to address the strain on data transmission and processing resulting from high-frequency AE sampling for monitoring crack leakage in pipeline welds. However, these methods focus on detecting and locating cracks and leaks in pipelines after they occur, limiting the capability to monitor the health condition of pipelines before failures occur.

In the frameworks of condition-based monitoring (CBM) and prognostics and health management (PHM) using CBM, an essential task is predicting the RUL. Predicting RUL involves estimating the duration over which a system or component can perform its function, which is crucial for decision-making in contingency mitigation [30]. Typically, such prediction involves two primary approaches: degradation model-based and historical data-based predictions [31]. Degradation model-based prediction relies on mathematical models representing degradation processes, providing insights into underlying mechanisms and facilitating proactive maintenance planning [32]. However, creating accurate models can be challenging due to real-world uncertainties and complexity [33]. Conversely, historical data-based methods estimate RUL using past run-to-fail data, lacking proactive insights but reflecting real-world failure scenarios [33], [34]. While degradation models offer accuracy and proactive maintenance potential, historical data-based methods offer simplicity and practicality with limited detailed degradation knowledge or extensive data.

Studies on data-based methods for pipeline RUL prediction have garnered widespread attention due to their feasibility. Shaik et al. [35] investigated the effects of corrosion on oil and gas industry piping systems, identifying factors influencing pipe longevity such as pressure, corrosion, wall thinning, and age. Subsequently, an artificial neural network was deployed to predict the RUL of pipelines before leakage based on inspection report data history from an oil and gas company in Malaysia. Xu et al. [36] used machine learning (ML) techniques to tackle the complexities of multi-dimensional corrosion monitoring data, aiming for intelligent corrosion prediction. They also highlighted the promising applications of deep learning (DL) methods in this domain. Priyanka et al. [37] introduced a digital twin-based framework employing ML and prognostics algorithms to analyze and to predict the risk probability rate of oil pipeline systems. They focused on pressure-based risk estimation for RUL evaluation and abnormal pressure detection through clustering methods. These RUL prediction methods primarily focus on recent ML/DL models to predict the lifespan of pipelines due to corrosion over time. Meanwhile, there is no research on predicting the RUL of pressurized pipelines where failures are caused by cracks or ruptures. Furthermore, a major limitation of ML/DL models trained on data involves data interpretation [38]. In these models, there is uncertainty in the relationship between input data and predicted output, reducing the certainty of predictions and the reliability of models.

The issue of reliability in ML/DL models has been highlighted in research on engineering prognostics because certainty in predictions is needed for accurate maintenance decisions. To address this drawback, explicit learning methods based on data have been proposed, known as similarity-based RUL prediction [39], [40]. These methods examine the similarity in degradation behaviors between the data under examination and historical data, predicting RUL based on those of the most similar candidates. Recently,

Lyu et al. [41] transformed historical data into local segments representing degradation events and employed a strategy to identify events similar to the current state. These identified segments served as references for RUL estimation, with a self-adaptive weight allocation method to enhance prediction performance. Another previous study [42] developed a multimodal degradation features and adjusted cosine similarity (ACS) method for RUL prediction. The method utilized empirical mode decomposition to separate global degradation and random fluctuations and employed slow feature analysis for local degradation features for enhanced similarity evaluation. Qiu et al. [43] introduced a new approach called the supervised multi-head self-attention autoencoder (SMSAE) to directly extract a health indicator (HI) from raw vibration signals. The proposed HI construction is used in a two-stage residual life prediction framework based on similarity. However, current research on similarity-based RUL prediction primarily focuses on machines and rarely considers pipelines.

The analyses above show the considerable lack of comprehensive research in monitoring and predicting the RUL of pressurized pipelines in industrial processes. This deficiency is the main motivation for the present study. Specifically, we harness the advantages of AE monitoring for assessment of health condition of pressurized pipelines. In this study, we for the first time propose a HI for pressurized pipeline systems to represent the current health stage of the system. The proposed indicator is derived from the cumulative crack-related AE-hit events, representing potential failure warnings, detected by a constant false alarm rate (CFAR) detector [44]. Subsequently, an enhanced data-based explicit RUL prediction method is suggested to overcome the limitations inexplicability imposed by the opaque nature of ML/DL models. Inspired by [41], the proposed method relies on the similarity between the current HI trajectory and the past HI segments to estimate the remaining operational time. The similarity of trajectories of the HI is measured using Euclidean distances within the introduced derivative convolutional domain (refer to Section II-B. for this definition). Afterward, these distances are weighted based on a data-adaptive fuzzy logic rule to allow all computed distances to be used with their corresponding similarity level. As the distance decreases, the similarity in trajectory increases, leading to a higher allocated weight corresponding to greater similarity in the RUL. Finally, the predicted RUL is the weighted sum of the corresponding RULs of the computed distances.

The main contributions of this research are summarized as follows:

- A novel health indicator for pressurized pipelines is introduced, constructed based on the accumulation of AE-hit events using the CFAR detection algorithm.
- An enhanced similarity-based RUL prediction method is proposed, using HIs from historical run-to-fail data. The similarity evaluation strategy is based on Euclidean distances in an introduced derivative convolutional domain and is weighted by a data-adaptive fuzzy rule.
- Validation experiments are conducted on a custom in-laboratory setup for pressurized pipes to verify the effectiveness and to compare the performance of the proposed method with others.

II. BACKGROUND CONCEPTS

A. CONSTANT FALSE ALARM RATE DETECTION

The CFAR is a classic signal detection algorithm used to detect targets in radar engineering. The advantage of the CFAR lies in its adaptability to signal variations without prior knowledge of the target waveform [44]. In the present study, the CFAR is implemented to perform AE-hit detection to identify crack events in the pipeline. The CFAR principle is straightforward: it estimates an adaptive threshold and produces a signal if this threshold is surpassed. The detection threshold (Th) for each cell is calculated using the background noise power level (P_n), estimated from neighboring cells as follows [44]:

$$Th = \alpha P_n \tag{1}$$

where α is a scaling factor called the threshold factor.

In CFAR detectors, the most common approach is cell averaging (CA-CFAR), which involves calculating P_n based on the average power of neighboring cells. However, to avoid the influence of the cell under test (CUT), cells (guard cells) directly adjacent to it are excluded (see Figure 1). Consequently, P_n is computed based on the remaining neighboring cells (training cells) as [44]:

$$P_n = \frac{1}{N} \sum_{i=1}^{N} x_i \tag{2}$$

where N is the number of training cells and x_i is the sample in the i-th training cell.

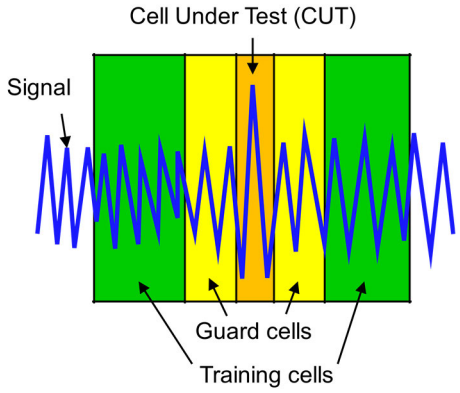

FIGURE 1. The relationships among the CUT, guard cells, and training cells.

As the value of α decreases, the threshold value decreases, leading to a higher false alarm rate, i.e., a higher probability of false detection of noise as a signal. Therefore, to determine an appropriate α value, practitioners limit the false alarm rate to a pre-defined level denoted as P_{fa} (probability of false alarm). With the CA-CFAR detector, the threshold factor can be written as follows [44]:

$$\alpha = N \left(P_{fa}^{-\frac{1}{N}} - 1 \right) \tag{3}$$

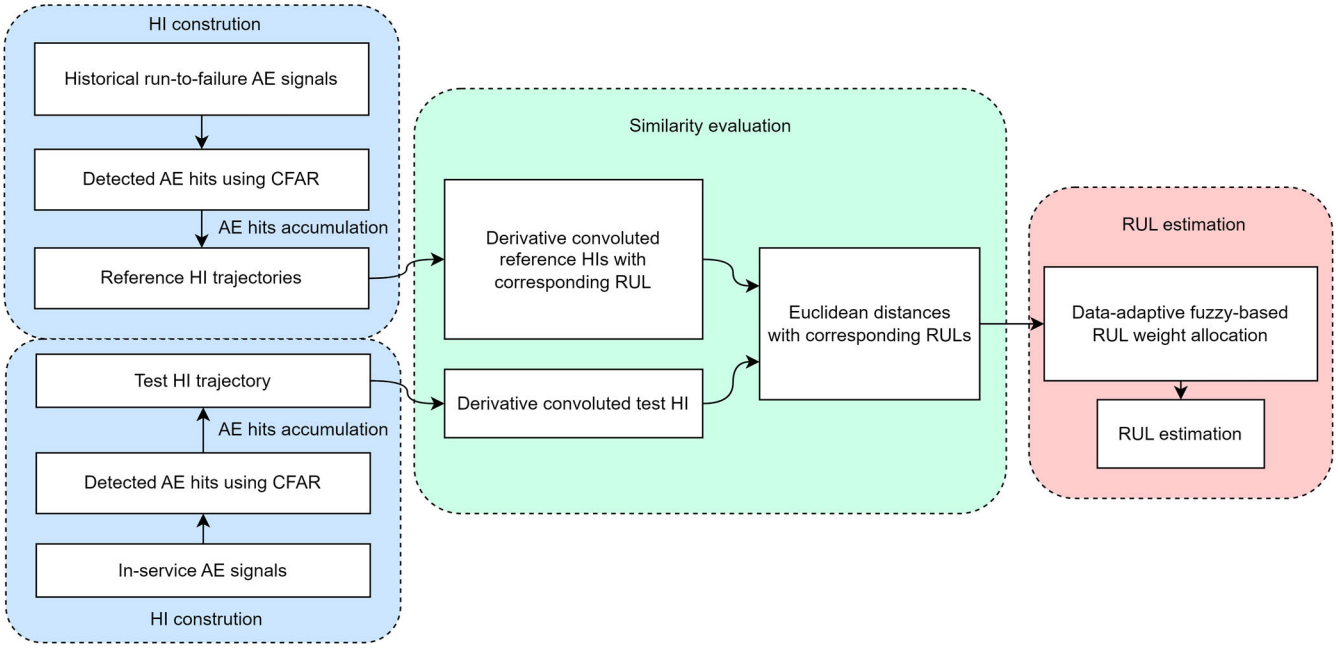

FIGURE 2. Flowchart of the proposed method.

B. SIMILARITY-BASED RUL PREDICTION

The first mature proposal of similarity-based RUL prediction was introduced in [45] and has been revisited in recent years due to its transparency surpassing ML/DL "black box" algorithms. Similarity-based RUL prediction comprises three fundamental steps: data collection and fusion, similarity assessment, and prediction aggregation [39]. In the first step, run-to-fail data are gathered from various sensors and fused to generate a singular representative index known as the HI [39]. Based on this HI, the system's condition or degree of degradation can be ascertained. Naturally, these HIs must satisfy certain criteria, such as monotonicity and trendability, to be meaningful for prognostics [46]. Monotonicity refers to the consistent direction of change in a variable with regard to another variable. This means that, as the health condition of a population improves or deteriorates, the indicator consistently moves in the same direction [47]. Meanwhile, trendability relates to the ability of an HI to capture and reflect trends in health outcomes over time. A health indicator should be sensitive to changes in health stage, allowing identification of patterns and trends [47]. The formulas for monotonicity and trendability are presented in (4) and (5), respectively:

$$Mon. = \frac{1}{N-1}\left|\sum_{i=1}^{N-1} sgn\left(x_{i+1} - x_i\right)\right| \tag{4}$$

$$Tren. = \left|cov\left(t_i, x_i\right)\right| \tag{5}$$

where N is the length of the HI trajectory, x_i is the i-th point of the trajectory and t_i is the corresponding time, sgn is the sign function and cov is the covariance.

In the second step, the in-service HI is compared with HIs present in the historical data to assess similarity. This process involves computing similar metrics and matching trajectories. Greater similarity implies more analogous patterns, indicating a closer resemblance in degradation trends, aiding in predicting the current in-service system trend. There are various types of distances commonly used to measure similarity, such as Euclidean and Mahalanobis distances, chosen based on the characteristics of the data. Without loss of generality, the Euclidean distance is considered in this study, and the formula for two points (x_1, y_1) and (x_2, y_2) is as follows:

$$D = \sqrt{(x_2 - x_1)^2 + (y_2 - y_1)^2} \tag{6}$$

Finally, in the third step, prediction of the RUL is determined based on the similarity distance from the previous step. Specifically, for each distance between the in-service HI and a reference HI, the similarity distance corresponds to a reference RUL value of the reference HI. Consequently, the in-service RUL typically is calculated either simply by selecting the RUL where the distance is minimal or by a weighted sum of the reference RULs. In this study, weights $weight_k$ are distributed to reference RULs RUL_k and the final predicted RUL is calculated as shown in (7), where M is the number of reference RULs:

$$RUL = \sum_{k=1}^{M} weight_k \times RUL_k \tag{7}$$

III. METHODOLOGY

A. OVERVIEW

This section provides an overview of the proposed method for predicting the RUL of pressurized pipelines. This section offers a preliminary description and outlines the main data flow, and the specific details regarding individual steps will be expounded upon in subsequent sections. Figure 2 illustrates the flowchart of the proposed method, comprising three primary blocks corresponding to three stages in

similarity-based RUL prediction: HI construction, similarity evaluation, and RUL estimation.

In the initial step, the HI construction block is tasked with generating trajectory lines that represent the health condition of the pipeline. These HIs are calculated by accumulating AE events/hits detected by CFAR, as they signify the severity of faults. The HI trajectory lines include reference trajectories constructed from historical run-to-fail data and test trajectories constructed from in-service data. Subsequently, these trajectory lines undergo similarity evaluation to identify similarities between the in-service and reference HIs. The degree of similarity is measured using Euclidean distances in the derivative convolutional domain, detailed further in subsequent sections. From this stage onwards, each computed distance is accompanied by a corresponding reference RUL value associated with the compared reference HI. In the third step, the RUL estimation block assigns weights to the distances and corresponding reference RULs based on their influence on the predicted RUL using data-adaptive fuzzy logic. Then, the predicted RUL is calculated as the sum of the weighted reference RULs.

B. HI CONSTRUCTION

In this study, we implement the CA-CFAR algorithm to detect AE events/hits in the monitored signals. Specifically, based on prior research experiences regarding crack detection in pipelines [45], the proposed parameter values for the CA-CFAR detector are as follows: the false alarm probability is maintained at 10^{-7}, a cell size of 500 points (0.5 ms) is used, with 10 guard cells and 20 training cells. Once the noise level is estimated using CA-CFAR, any CUT surpassing the energy threshold is considered to contain AE information. An independent AE event is defined as a group of consecutive CUTs containing AE information. Figure 3 illustrates a segment of the signal in this study, with dotted boxes highlighting the detection of independent AE events/hits. Subsequently, the proposed HI is constructed by totaling cumulatively the number of AE hits detected over time.

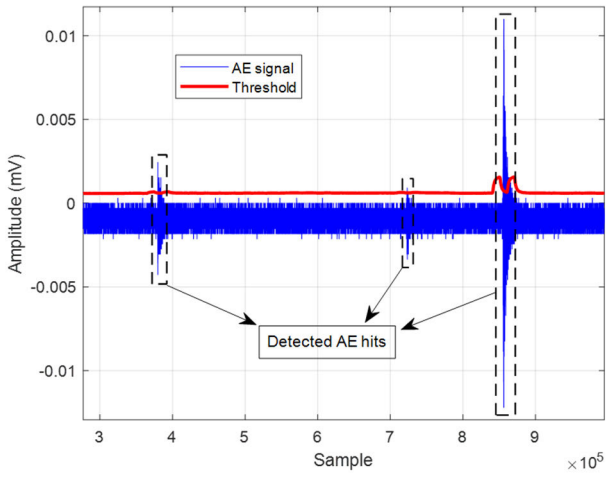

FIGURE 3. Illustration of AE hits (in dotted boxes) detected by the CFAR algorithm.

C. SIMILARITY EVALUATION

The evaluation of similarity is conducted using the HIs introduced in the previous section. Based on our observations, industrial processes often exhibit repetitive patterns following predetermined working condition profiles, rendering them conducive for similarity assessment. However, the actual trajectories of pipeline health conditions between these instances are never entirely identical. As the AE count in the HI experiences abrupt shifts each time pressure alterations cause material bond ruptures, these patterns become critical for assessing similarity. Therefore, to augment information derived from the working condition profile, we introduce the derivative convolution operation to extract information regarding the temporal changes in the count of AE events:

$$DC\,(x, n) = x * saw_n(t) \tag{8}$$

where $*$ signifies the convolution operation, x is the original signal transformed, and saw_n is the n-point sawtooth function ($n = 1000$ in this research):

$$saw_n(t) = \begin{cases} 1 - \frac{2t}{n-1}, & t = 0, \ldots, n-1 \\ 0, & otherwise \end{cases} \tag{9}$$

The ensuing task involves comparing whether the test HI exhibits patterns that resemble reference HIs. Given the variations in the lengths of HI trajectories, we adopted the concept of multi-local segments from [41] to segment the reference HIs into sections equivalent in length to the test HI. Specifically, we partition the reference HI into segments with a step of 100,000 points (0.1 s) to retain inter-segment associations. Then, the test HI is compared with reference HI segments based on Euclidean distances within the derivative convolutional domain. For every segmented reference HI, there is a corresponding RUL, denoting the remaining operational duration from the segment's endpoint. These RULs are referred to as reference RULs for convenience in subsequent discussions about RUL prediction.

D. RUL ESTIMATION

In the final step of the proposed method, predictions about the RUL of in-service HIs are based on their similarity levels with the reference HIs. In many similarity-based methods, this is accomplished by assigning weights to the measured distances of similarity and then computing their sum with corresponding weights. In this study, the first step is to assess the importance of each distance measure of similarity, accomplished by introducing a weight allocation scheme based on fuzzy logic. While smaller distances should be associated with larger weights, and vice versa, attention must be paid to the correlations between the weights. However, this is somewhat challenging as we do not have knowledge of the true distribution of distance variables. Therefore, in this study, the variables are assumed to follow a normal distribution. A Gaussian membership function, adapted to the observed data, is utilized to calculate weights for the similarity distance variables, as follows:

$$w\,(x) = \exp\left(-\frac{x^2}{2\sigma^2}\right) \tag{10}$$

where x represents the input distance value, and σ stands for the standard deviation. With this membership function, $x = 0$ corresponds to the highest similarity, yielding the highest weight. Meanwhile, the adaptive parameter σ is computed based on the standard deviation of the observed data as defined in equation (11), where $\bar{x}$ represents the mean of the distance values x_k, and M denotes the number of these values. Figure 4 presents the Gaussian membership function with a mean of 0 and a standard deviation of 1.

$$\sigma = \sqrt{\frac{1}{M-1}\sum_{k=1}^{M}(x_k - \bar{x})^2} \tag{11}$$

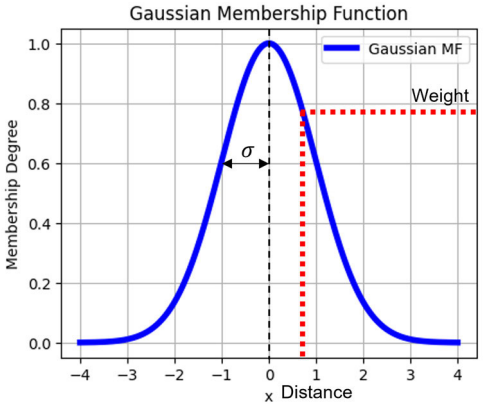

FIGURE 4. The Gaussian membership function.

Once the weights are assigned to the distance measures, they are used to calculate the ultimate RUL. For each reference distance, there exists a corresponding reference RUL. Thus, the weight of each reference distance is multiplied by its corresponding reference RUL, as specified in the following formula:

$$RUL = \sum_{k=1}^{M} \frac{w_k}{\sum_{j=1}^{M} w_j} \times RUL_k \tag{12}$$

where M represents the number of distance measures, and RUL_k and w_k respectively denote the reference RUL and its corresponding weight for its reference distance.

IV. EXPERIMENTAL SETUP

This section presents the organization of validation experiments, including the setup of the test bed, data collection scenarios, evaluation criteria, and a comparative analysis of the experimental results.

Figure 5 depicts the schematic design of a test bed system for simulating industrial pressurized pipeline systems. The system includes a cylindrical pipe segment (the test pipeline), measuring 2000 mm in length, which is marked and capped with flanges at both ends. Accompanying this is a water tank system and a pump to provide a flow of fluid into one end of the pipe and out the other. The pump and two valves are software-controlled to generate the desired pressure, measured by two pressure sensors (PS1 and PS2) at the ends of the pipe segment. To monitor crack events using acoustic emissions, four AE sensors (labeled S5, S6, S7, and S8) are mounted at opposite ends of the pipe segment (refer to Figure 5). All sensors (pressure, AE) and actuation mechanisms (the pump and valves) are controlled and monitored through a data acquisition (DAQ) unit connected to a computer and storage.

Figure 6 shows an actual image of the test bed system located in the laboratory. In addition to the described components, the actual system includes two supports/props to brace the pipe segment. To ensure safety, the experimental area is segregated from the control and monitoring area. The technical specifications of the equipment used in the test bed system are detailed in Table 1.

TABLE 1. Testbed equipment specifications.

Equipment	Specification	Value	Unit
Test pipeline	Material	Carbon steel	-
	Length	2000	mm
	Thickness	4.85	mm
	Outer diameter	165.2	mm
AE sensor	Type	R15I-AST	-
	Peak sensitivity	109	dB
	Resonance frequency	150	kHz
	Operating frequency	50 to 400	kHz
	Operating temperature	-35 to 75	°C
DAQ	Type	EXPRESS-8	-
	Manufacturer	MITRAS	-

The data acquisition scenario is designed to describe a pressure increase process typical in industrial operations. Accordingly, the pipeline pressure is increased gradually in the following sequence: initially initiated at 0 bar, increased to 50% of the pressure design (Pd) for the next 10 minutes, followed by 10 minutes at 65% Pd, and then 10 minutes at 80% Pd. The pressure is maintained at 100% Pd for the subsequent 30 minutes. After that, the pressure is increased further as 5 minutes at 200% Pd, 5 minutes at 400% Pd, and then 5 minutes at 600% Pd. Thereafter, the pressure is increased incrementally by 100% Pd every 5 minutes until the pipeline ruptures. Illustrations of the pressure increment process and an image depicting a ruptured pipeline are shown in Figure 7. Considering that the AE signal frequency in steel ranges from 100 to 300 kHz [46], the sampling rate for the AE sensors is set at 1 MHz, adhering to the Nyquist–Shannon sampling theorem.

The four experimental pipes are designated as B, C, D, and E. The entirety of data from each sensor for a specific pipe and location is stored independently in a single data file. The data structure for our validation experiments is planned as follows: the data files obtained from AE sensors 7 and 8 of all four test pipes are used as historical reference data to construct reference HIs. The remaining data files collected from AE sensors 5 and 6 are utilized as test data resembling in-service data. Hence, there are eight reference files denoted

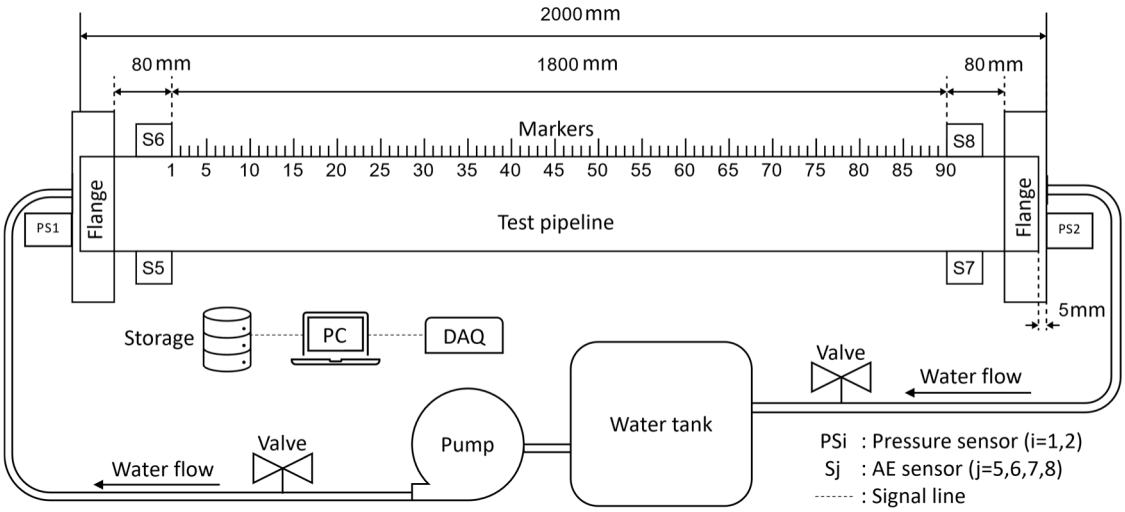

FIGURE 5. Schematic design of the experimental testbed.

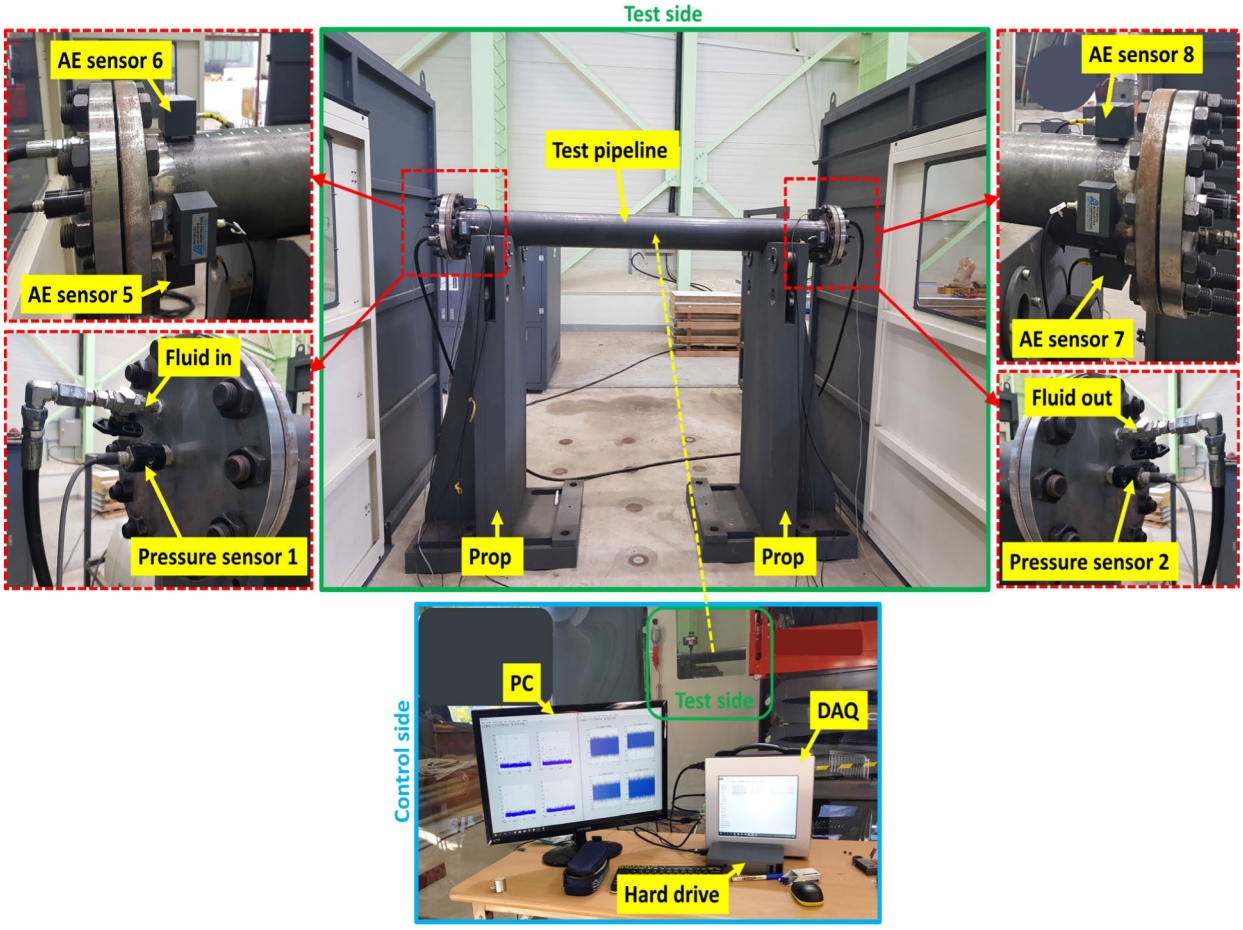

FIGURE 6. Photographs of the experimental testbed setup.

as B7, B8, C7, C8, D7, D8, E7, and E8 and eight test files denoted as B5, B6, C5, C6, D5, D6, E5, and E6. For each test file, to simulate the in-operation state of the pipeline, segments of data from the initial stage are extracted, ranging

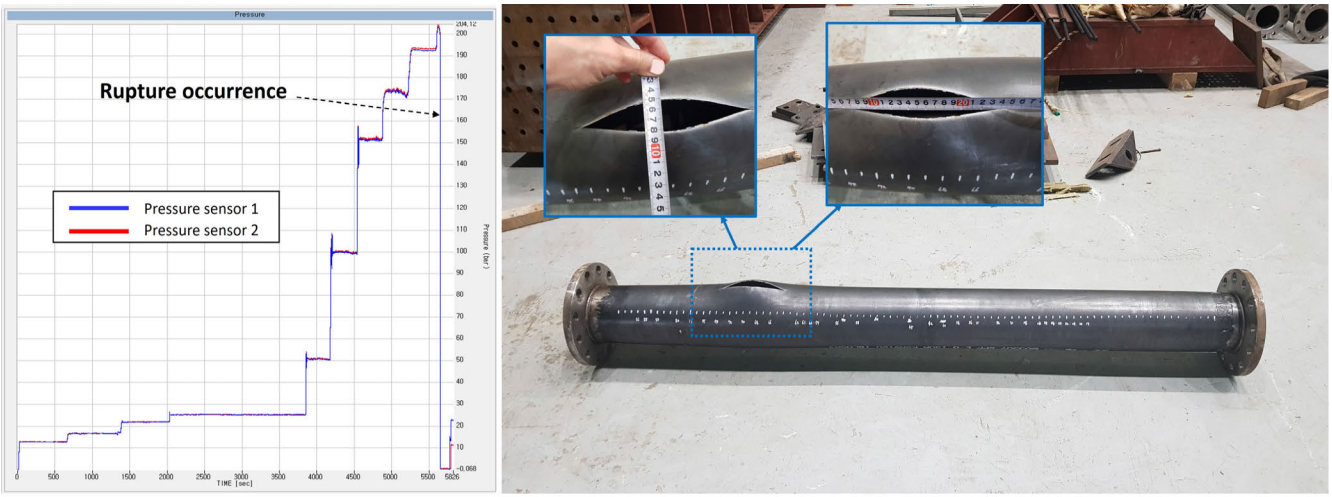

FIGURE 7. Illustration of (a) the pressure increment process and photographs of (b) a ruptured pipeline.

from 10% to 90% at intervals of 5% of the total operating time of that pipeline. These data segments will be used as in-service data for the proposed method to predict their RULs.

The criteria for evaluating the accuracy of the predicted RUL in the experiments include the mean absolute error (MAE), root mean square error (RMSE), and PHM score [47]. The first two criteria are familiar and fundamental measures commonly used in assessing overall accuracy. The formula for the MAE is presented in (13), and that for the RMSE in (14):

$$MAE = \frac{1}{N}\sum_{k=1}^{N}\left|\hat{y}_k - y_k\right| \tag{13}$$

$$RMSE = \sqrt{\frac{1}{N}\sum_{k=1}^{N}\left(\hat{y}_k - y_k\right)^2} \tag{14}$$

where N denotes the number of predictions, and y_k and $\hat{y}_k$ respectively denote the real (true) RUL and predicted RUL. The PHM score demonstrates that predictions in the early stages typically are more challenging and less critical than those in the later stages. Therefore, the formula for the PHM score involves assigning weights to predictions at different times r_k (unit: % of total operating time), as shown in (15):

$$PHM = \sum_{k=1}^{N}\frac{r_k}{\sum r_k}\times\left|\hat{y}_k - y_k\right| \tag{15}$$

V. RESULTS AND DISCUSSION

In this section, we begin by assessing the proposed HI to verify its effectiveness in representing and predicting the health condition of pressurized pipelines. Subsequently, experiments on predicting the RUL using our dataset are carried out to assess the accuracy of the proposed method. Additionally, uncertainty assessments in the predictions are evaluated through uncertainty testing experiments. Alongside the verification experiments, comprehensive comparisons are performed to strengthen the achieved results of this study.

A. HEALTH INDICATOR ASSESSMENT

In this section, the proposed HI is examined and evaluated to demonstrate its effectiveness in addressing the prognostics problem. Figure 8 presents a visualization of the HI trajectories across all data files over the entire lifetime, including HI reference trajectories (in blue) and HI test trajectories (in red). These HI trajectories exhibit varying lifespans and an increasing trend due to computation based on the cumulative number of AE hits caused by cracks, which increase over time.

Quantitative assessment of the quality of these HIs requires computation of metrics related to monotonicity and trendability, as outlined in Section II-B. These indices range between 0 and 1, with values closer to 1 indicating a higher potential for application in prognostic problems. Furthermore, to compare the proposed HI with other HIs built on traditional statistical features, we extracted features from AE signals, including root mean square (RMS), mean, standard deviation, kurtosis, skewness, crest factor, and entropy. Subsequently, traditional HIs were defined as trajectories of these features over the lifetime and were computed every second.

Figure 9 contrasts the monotonicity and trendability of the proposed and traditional HIs. First, focusing on monotonicity, a significant difference is evident between the proposed HI and the others. Specifically, while the proposed HI exhibits a remarkably high monotonicity of 0.94, the mean and entropy are only 0.16 and 0.13, respectively; the remaining indices do not surpass 0.01. The reason behind this is that traditional HIs are less affected or altered by a pressure increase. The difference arises during pressurization due to the appearance of AE hits, which rapidly affect the signal features, hindering their detection.

Regarding trendability, as it correlates the HI amplitude with time, it shows some improvement compared to monotonicity. Specifically, the proposed HI attains an absolute trendability of 1.00, entropy of 0.97, and mean trendability

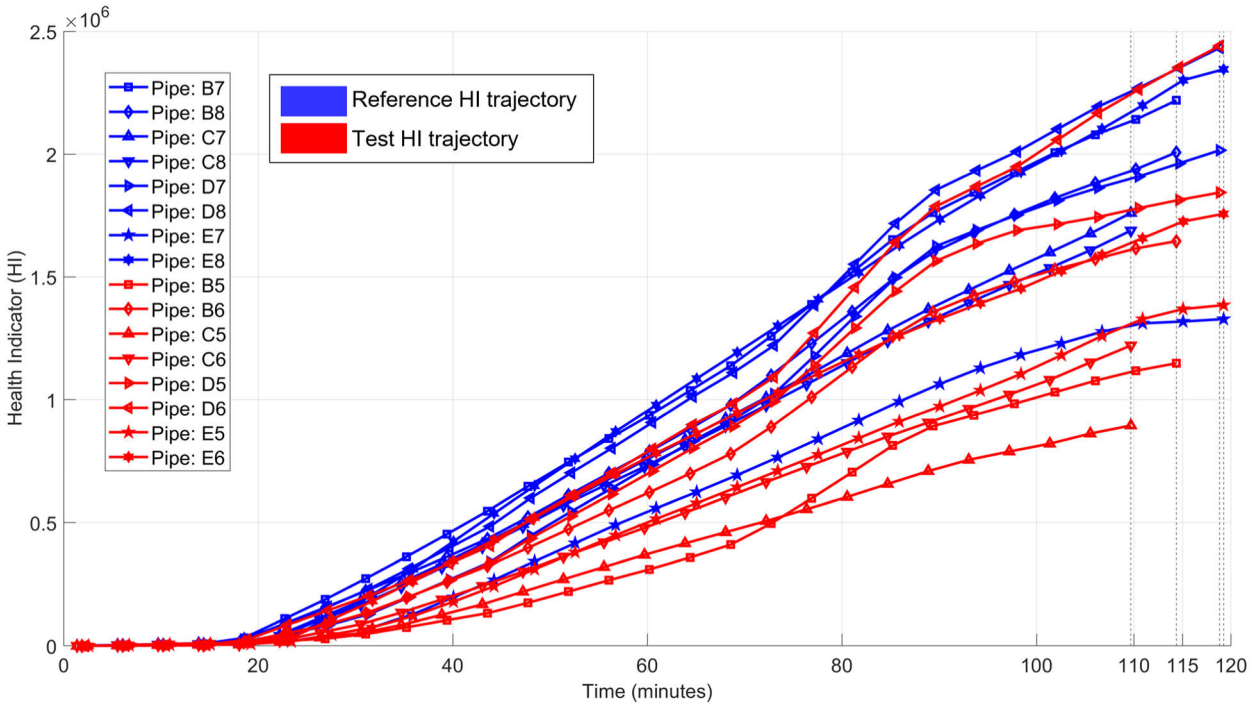

FIGURE 8. Plots of the proposed HI trajectories.

of 0.64. The RMS and standard deviation are 0.32 and 0.35, respectively, while the remaining variables are less than 0.1. Although traditional HIs can be used to predict the RUL, their nature makes them insensitive to signs of failure, particularly regarding AE hits, limiting their reliability. Conversely, the proposed HI aligns with the context and presents excellent quantitative metrics, surpassing traditional HIs to serve as an indicator for the health of pressurized pipelines.

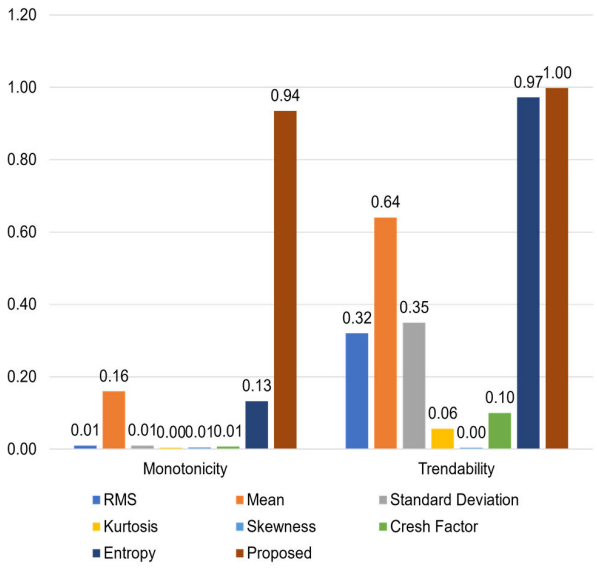

FIGURE 9. Monotonicity and trendability comparisons between the proposed and traditional HIs.

Although the proposed HI can be used to predict the RUL for a pressurized pipeline, its value range is not consistent across HIs. Thus, relying solely on conventional distance measures to gauge similarity is insufficient. For instance, Figure 10 illustrates four HI trajectories (dashed lines) from sensors 5 and 7 on pipes B and C, along with their mappings in the derivative convolutional domain (solid lines). Notably, when two HIs from the same pipe share the same RUL, the similarity between sensor 5 on pipe B and sensor 5 on pipe C or sensor 7 on pipe C can be difficult to distinguish due to their proximity in the two-dimensional space.

Considering the derivative convolutional domain (the solid lines in Figure 10) proposed in section III-C., similar patterns between two truly analogous HIs, sensor 5 (pipe B) and sensor 7 (pipe B), easily are observable. These patterns stem from the same pressure profiles of the sensors, accurately depicting the resemblance between two HIs on the same pipe. Therefore, measuring similarity within this domain can provide accurate insights into the resemblance between two HIs, enabling precise predictions of the RUL with high accuracy. It is evident that the proposed method lays the foundation for determining similarities in the derivative convolutional domain. In subsequent experiments, various similarity calculation methods are evaluated to validate the effectiveness of the proposed approach.

B. RUL PREDICTION PERFORMANCE

This section presents the performance of the proposed method on test data B5, B6, C5, C6, D5, D6, E5, and E6, encompassing predictions of the RUL and accuracy

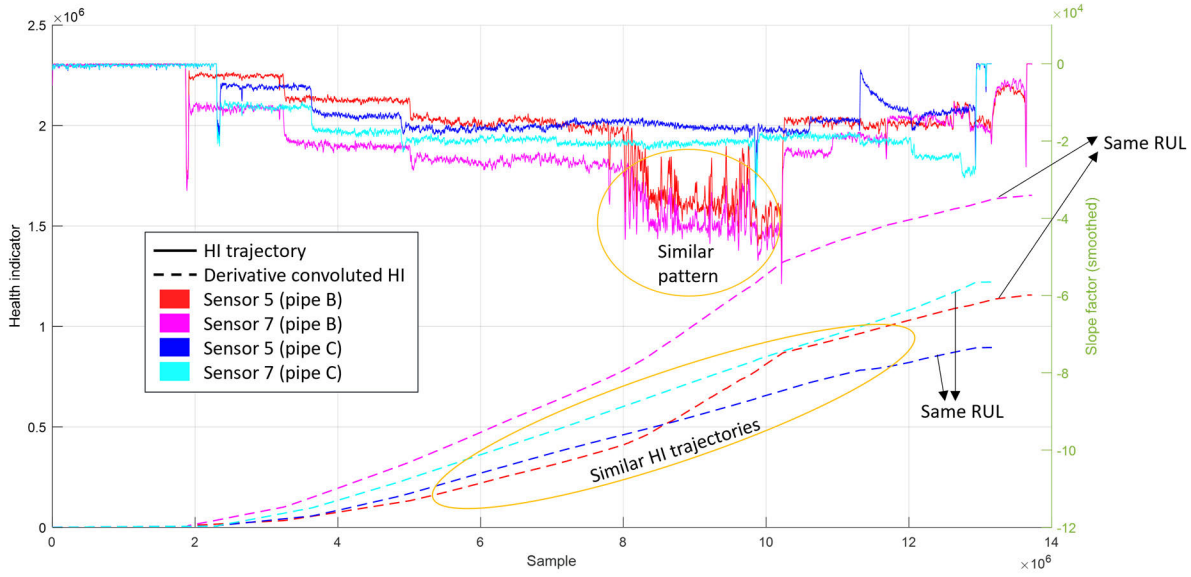

FIGURE 10. Illustration of four HI trajectories along with their mappings in the derivative convolutional domain.

metrics. Moreover, to demonstrate the superiority of the proposed method over others, comparative experiments were conducted. Specifically, the examined methods all directly estimated RUL based on the proposed HI but differed in their similarity evaluation approaches, including the Euclidean distance method (Euclidean method), the Euclidean method with weights assigned according to a proposed fuzzy logic scheme (weighted Euclidean method), and the multiple local similarities method (MLS method) in [41].

The predicted RUL results of the proposed method and other examined methods are presented in Figure 11. Initially, the compared methods relatively accurately predict RUL in an intuitive manner, especially those based on the Euclidean distance. This achievement is attributed to the selection of a suitable HI for the problem. Second, these methods exhibit a tendency for increased prediction errors in the early lifetime due to the scarcity of available information during that period. As expected, accuracy gradually improves as more information becomes available. The MLS method appears to be an exception, as it frequently deviates from the real RUL trajectory in the late stages.

In most tests, the RUL predicted by the proposed method closely aligns with the real RUL line, especially in the latter periods. This observation is noticeable in the tests of B5, B6, C5, C6, and E6. In contrast, the Euclidean method shows results that run parallel to the true RUL, which is unfavorable due to its misinterpretation of the test HI to resemble a reference. The weighted Euclidean method produces more accurate predictions in the latter stages compared to the Euclidean method. However, the predictions from the MLS method intersect the real RUL line, leading to substantial deviations in both initial and final predictions from the real values. Comparing these methods, the proposed method qualitatively is superior. These initial observations, discussions, and comparisons aim to demonstrate the effectiveness and superiority of the proposed method in predicting the RUL of pressurized pipes. The quantitative comparisons will further elucidate the superiority of the proposed method.

Table 2 displays the comparative analysis of mean MAE across different methods employed for testing pipes. Notably, the proposed method showcases remarkable efficiency, yielding the lowest MAE values across most test pipes. Specifically, for pipes B5, B6, C5, C6, and E6, the proposed method recorded substantially lower errors of 2.60, 4.46, 4.05, 2.91, and 5.44, respectively, compared to other methodologies. Meanwhile, the Euclidean method achieves the smallest MAE in pipes D5, D6, and E5 with respective values of 5.00, 4.64, and 4.69, as observed in Figure 11. In these tests, the proposed method achieves the second-best values of 6.83, 6.89, and 7.53. Both the weighted Euclidean and MLS methods exhibit MAE values inferior to the other methods. This suggests the superior predictive accuracy and reliability of the proposed method in estimating the RUL of these pipes, underscoring its potential for enhanced performance in this domain.

In Table 3, the RMSE among various methods applied to test pipes is presented. The proposed method consistently demonstrates favorable RMSE values across multiple test pipes, as in Table 2. Specifically, for pipes B5, B6, C5, C6, and E6, the proposed method shows notably lower RMSE values at 4.37, 5.27, 4.35, 3.40, and 5.91, respectively, compared to other methodologies. The Euclidean method continues to showcase its performance with RMSE values of 5.00, 6.21, and 4.82 for pipes D5, D6, and E5, respectively. In these tests, the proposed method achieves the second-best values of 8.22, 8.54, and 8.32. The other two methods demonstrate inferior performance, as seen in the previous Table 2. These further underscore the superiority of the proposed method, highlighting its capability in estimating the RUL of pressurized pipelines.

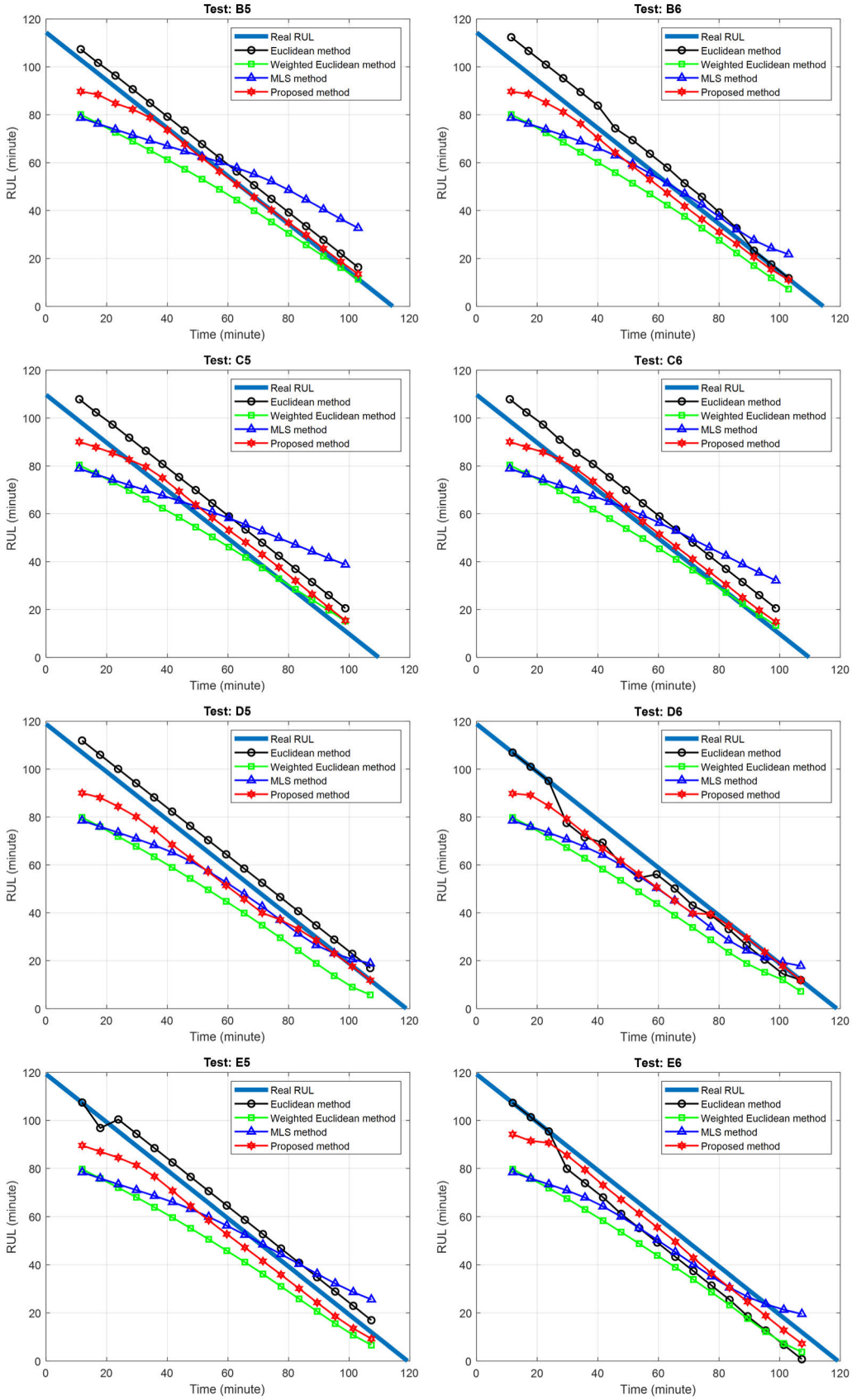

FIGURE 11. Performance of the proposed method in RUL prediction and comparison with other methods.

Table 4 presents the comparative analysis of the PHM scores across various methods applied to test pipes. Notably, the proposed method consistently exhibits superior performance with notably lower PHM scores across multiple test pipes. Specifically, for pipes B5, B6, C5, C6, D5, and E6, the proposed method demonstrates substantially lower PHM scores of 1.47, 3.35, 4.07, 2.74, 4.71, and 4.95, respectively, in comparison to alternative methodologies. These findings accentuate the effectiveness of the proposed method in achieving more accurate prognostic assessments, signifying its potential for enhanced reliability in predicting the health and prognosis of pipes.

The evaluation of the three distinct performance metrics of the MAE, RMSE, and PHM scores across various methodologies in pipes B5, B6, C5, C6, D5, D6, E5, and E6 underscores the remarkable efficacy of the proposed method. Obviously, the proposed method consistently outperforms other methodologies across all three assessments. All the best values per test (the smallest values in each row) in the tables are highlighted in red, while the second-best values are highlighted in blue. In all test pipes, the proposed method predominantly occupies positions with the best and second-best positions. The Euclidean method frequently secures the second-best position, while the other two methods have few strengths to consider. Collectively, these results underscore the exceptional performance of the proposed method, highlighting its consistent and superior predictive capabilities in estimating pipe remaining lifetime compared to alternative methodologies.

TABLE 2. Mean absolute error comparison.

Test pipe	Euclidean method	Weighted Euclidean	MLS method	Proposed method
B5	**4.80**	9.68	12.87	**2.60**
B6	**6.07**	11.64	8.22	**4.46**
C5	9.49	**6.84**	13.31	**4.05**
C6	9.39	**6.84**	11.19	**2.91**
D5	**5.00**	15.77	10.45	**6.83**
D6	**4.64**	15.89	11.69	**6.89**
E5	**4.69**	15.03	10.97	**7.53**
E6	**8.59**	16.82	11.59	**5.44**

C. UNCERTAINTY EVALUATION

In addition to evaluating the accuracy of RUL predictions, uncertainty also is assessed as a prognostic algorithm. Uncertainty is defined as the range of predicted values that the model considers correct. Evidently, the smaller is the range of predicted values, the smaller is the uncertainty, meaning a greater certainty of prediction. To compute uncertainty, the model must provide output predictions that include the probability of their occurrence. In this case, models with weighted predictions can meet this requirement, where the weights are scaled to resemble probability values. In this section, the proposed method, the weighted Euclidean method, and the MLS method are introduced to conduct an assessment and comparative analysis.

TABLE 3. Root mean square error comparison.

Test pipe	Euclidean method	Weighted Euclidean	MLS method	Proposed method
B5	**4.80**	11.93	14.56	**4.37**
B6	**6.86**	12.92	10.82	**5.27**
C5	9.49	**8.84**	15.42	**4.35**
C6	9.39	**8.92**	12.79	**3.40**
D5	**5.00**	16.79	13.20	**8.22**
D6	**6.21**	17.09	13.89	**8.54**
E5	**4.82**	16.35	13.73	**8.32**
E6	**9.48**	17.66	14.00	**5.91**

TABLE 4. PHM score comparison.

Test pipe	Euclidean method	Weighted Euclidean	MLS method	Proposed method
B5	**4.84**	6.30	12.97	**1.47**
B6	**4.60**	8.94	5.85	**3.35**
C5	9.52	**4.39**	15.20	**4.07**
C6	9.47	**4.17**	11.99	**2.74**
D5	**5.00**	12.97	6.90	**4.71**
D6	**4.22**	12.84	8.26	**4.57**
E5	**4.93**	11.92	8.30	**6.08**
E6	10.05	14.24	**8.04**	**4.95**

The next step is to determine the range of values where the model is most certain, i.e., when the probability of failure reaches a predefined threshold, set at 90% in this study. To achieve this, the probability distributions of the predictions need to be estimated, which commonly is accomplished using kernel density estimation (KDE) methods [48]. This method is a non-parametric estimation technique that does not require prior knowledge about the probability distribution of a population. The kernel density estimator is an estimated probability function for a random variable x, defined as follows [48]:

$$\hat{f}_h(x) = \frac{1}{Nh} \sum_{k=1}^{N} K\left(\frac{x - x_k}{h}\right) \tag{16}$$

where N is the number of samples, K is the kernel smoothing function (Gaussian), and $h$is the bandwidth estimated by Silverman's rule of thumb [47].

Figure 12 illustrates the probability density function estimation of the predicted RUL associated with three examined methods in tests B, C, D, and E (sensor 6) at the 70% lifetime mark. Additionally, the range of values where the prediction probability reaches 90% is highlighted in green and referred to as the certainty zone. Notably, the accuracy of the predictions, depicted by the proximity between the predicted RUL (red line) and the real RUL (blue line), does not inherently signify the model confidence level. For instance, in test C, while

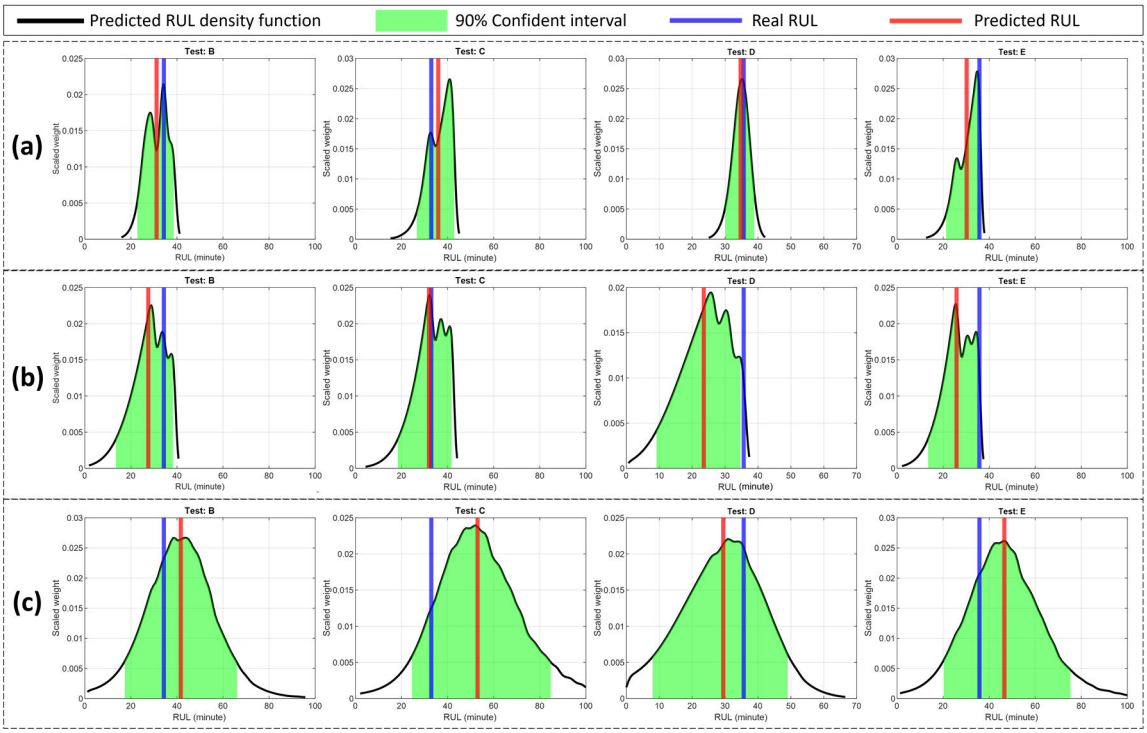

FIGURE 12. Uncertainty evaluation at 70% of the lifetime using: (a) the proposed method, (b) weighted Euclidean method, and (c) MLS method.

the weighted Euclidean method exhibits higher accuracy than the proposed method, it also displays greater uncertainty, as indicated by a narrower certainty zone.

Overall, uncertainty is relatively consistent across methods, as indicated by the width of the certainty zone. Specifically, the weighted Euclidean method displays uncertainty ranging from 21.2 to 36.5 minutes, and that of the MLS method ranges from 48.4 to 60.0 minutes. In contrast, the proposed method demonstrates lower uncertainty than the other two methods, with only approximately 12.3 to 16.3 minutes of uncertainty. This superior certainty likely is attributable to the meticulous selection of similarity metrics and appropriate weight allocation. The proposed method selectively prioritizes smaller similarity distances, effectively diminishing the impact of larger distance values. This showcases the promising potential for applications involving the prediction of RUL in pressurized pipes, particularly within industries demanding high reliability, such as the energy and chemical sectors.

The above observations clearly indicate that the proposed method exhibits the smallest mean uncertainty among all three methods. Specifically, in test pipes B5, D5, and D6, the mean uncertainty of the proposed method reached the lowest values of 8.68, 7.32, and 4.49 minutes, respectively. In contrast, the figures for the weighted Euclidean method ranged higher from 16.83 to 20.27 minutes, indicating a higher level of uncertainty compared to the proposed method. The MLS method displayed the highest uncertainty, ranging from 34.59 to 59.97 minutes on average. Consequently, the relative stability of uncertainty is noticeable among the methods. This reveals that the robustness of the proposed model's certainty is superior to the other two methods. This achievement can be attributed to the appropriateness of the employed similarity metrics and weight allocation mechanisms.

TABLE 5. Uncertainty comparison.

Test pipe	Weighted Euclidean	MLS method	Proposed method
B5	16.83	55.39	8.68
B6	20.27	42.21	13.47
C5	18.13	59.97	14.00
C6	20.08	53.94	15.48
D5	19.00	37.21	7.32
D6	18.72	34.59	4.49
E5	17.38	47.73	13.41
E6	18.78	39.83	11.10

VI. CONCLUSION

Pressurized pipeline systems play a critical role in industrial plants, and accurately predicting their RUL is imperative for pipeline health management. This research proposed a method to predict the RUL of pressurized pipelines in industrial processes based on acoustic emissions. A novel HI was introduced based on accumulated AE hits detected from material crack-induced events using the CA-CFAR algorithm. The proposed method relied on the learned similarity from historical HI trajectories to predict the RUL for the current HI. Similarity was measured using Euclidean distance in the derivative convolutional domain of the HI

trajectories. Finally, an adaptive fuzzy logic-based weighting distribution assigned weights for the similarity distances to estimate the RUL.

The efficacy of the proposed method was validated through experiments conducted on a testbed for pressurized pipelines in the laboratory. The experimental results revealed that the proposed method achieved high accuracy outperforming the other methods, as measured by the MAE, RMSE, and PHM scores. Furthermore, experiments testing the uncertainty of RUL predictions based on the KDE probability density estimation were conducted. The experimental outcomes affirmed that the proposed method achieved lower uncertainty compared to the other methods. These findings again confirmed the effectiveness and reliability of the proposed RUL prediction method for pressurized pipelines. However, it does not provide information on the exact location coordinates of cracks. Moreover, pipeline cracks can result from various factors such as fatigue, corrosion, and natural hazards, which remain undetermined. In the future, we will explore enhancing our method to include accurately locating and identifying the causes of cracks.

REFERENCES

[1] D. C. Rennels, *Pipe Flow: A Practical and Comprehensive Guide*. Hoboken, NJ, USA: Wiley, 2022.

[2] X. Chen, Z. Wu, W. Chen, R. Kang, S. Wang, H. Sang, and Y. Miao, "A methodology for overall consequence assessment in oil and gas pipeline industry," *Process Saf. Prog.*, vol. 38, no. 3, Sep. 2019, Art. no. e12050, doi: 10.1002/prs.12050.

[3] M. V. Biezma, M. A. Andrés, D. Agudo, and E. Briz, "Most fatal oil & gas pipeline accidents through history: A lessons learned approach," *Eng. Failure Anal.*, vol. 110, Mar. 2020, Art. no. 104446, doi: 10.1016/j.engfailanal.2020.104446.

[4] H. Krechkovska, O. Student, O. Zvirko, M. Hredil, L. Svirska, I. Tsybailo, and P. Solovei, "Substantiation of the critical structural and mechanical state of low-alloy heat-resistant steel from steam pipelines of thermal power plant," *Eng. Failure Anal.*, vol. 150, Aug. 2023, Art. no. 107359, doi: 10.1016/j.engfailanal.2023.107359.

[5] H. V. Krechkovs'ka, O. Z. Student, and H. M. Nykyforchyn, "Diagnostics of the engineering state of steam pipelines of thermal power plants by the hardness and crack resistance of steel," *Mater. Sci.*, vol. 54, no. 5, pp. 627–637, Mar. 2019.

[6] J. J. McKetta and W. A. Cunningham, *Encyclopedia of Chemical Processing and Design: Volume 37—Pipeline Flow: Basics to Piping Design*. New York, NY, USA: CRC Press, Jan. 2022.

[7] N. S. Zakaria, Z. M. A. Merican, and M. F. Hamza, "Performance and critical issues of polymer liners in pipeline industry: A review," *Mater. Today, Proc.*, vol. 16, pp. 2389–2397, Jan. 2019, doi: 10.1016/j.matpr.2019.06.143.

[8] Z. Ahmad, T.-K. Nguyen, A. Rai, and J.-M. Kim, "Industrial fluid pipeline leak detection and localization based on a multiscale mann-whitney test and acoustic emission event tracking," *Mech. Syst. Signal Process.*, vol. 189, Apr. 2023, Art. no. 110067, doi: 10.1016/j.ymssp.2022.110067.

[9] M. F. Siddique, Z. Ahmad, N. Ullah, and J. Kim, "A hybrid deep learning approach: Integrating short-time Fourier transform and continuous wavelet transform for improved pipeline leak detection," *Sensors*, vol. 23, no. 19, p. 8079, Sep. 2023, doi: 10.3390/s23198079.

[10] D.-T. Nguyen, T.-K. Nguyen, Z. Ahmad, and J.-M. Kim, "A reliable pipeline leak detection method using acoustic emission with time difference of arrival and Kolmogorov–Smirnov test," *Sensors*, vol. 23, no. 23, p. 9296, Nov. 2023, doi: 10.3390/s23239296.

[11] N. Bond, R. Symonds, and R. Hughes, "Pressurized chemical looping for direct reduced iron production: Carbon neutral process configuration and performance," *Energies*, vol. 15, no. 14, p. 5219, Jul. 2022, doi: 10.3390/EN15145219/S1.

[12] P. Akbari, C. D. Copeland, S. Tuchler, M. Davidson, and S. V. Mahmoodi-Jezeh, "Shock wave heating: A novel method for low-cost hydrogen production," in *Proc. ASME Int. Mech. Eng. Congr. Expo.*, Jan. 2022, pp. 1–23, doi: 10.1115/imece2021-69775.

[13] Y. Songtao, W. Ningning, W. Haijun, and Z. Mengxin, "Numerical simulation of leakage characteristics of pressurized water reactor nuclear power plant," *Nucl. Power Eng.*, vol. 2021, no. 3, pp. 32–37, Jun. 2021, doi: 10.13832/J.JNPE.2021.03.0032.

[14] C. H. Lin and Y. M. Ferng, "Predictions of hydrodynamic characteristics and corrosion rates using CFD in the piping systems of pressurized-water reactor power plant," *Ann. Nucl. Energy*, vol. 65, pp. 214–222, Mar. 2014, doi: 10.1016/j.anucene.2013.11.007.

[15] J. Modisette and G. Hanmer. (2021). *Simulation of Rapid Transients in Gas Pipelines for ESD Valve Design*. Accessed: Dec. 18, 2023. [Online]. Available: https://onepetro.org/PSIGAM/proceedings-abstract/PSIG21/All-PSIG21/PSIG-2107/463605

[16] Z. Liang, D.-S. Jeng, and J. Liu, "Combined wave–current induced seabed liquefaction around buried pipelines: Design of a trench layer," *Ocean Eng.*, vol. 212, Sep. 2020, Art. no. 107764, doi: 10.1016/j.oceaneng.2020.107764.

[17] J. Latif, M. Z. Shakir, N. Edwards, M. Jaszczykowski, N. Ramzan, and V. Edwards, "Review on condition monitoring techniques for water pipelines," *Measurement*, vol. 193, Apr. 2022, Art. no. 110895, doi: 10.1016/j.measurement.2022.110895.

[18] Y. Yu, A. Safari, X. Niu, B. Drinkwater, and K. V. Horoshenkov, "Acoustic and ultrasonic techniques for defect detection and condition monitoring in water and sewerage pipes: A review," *Appl. Acoust.*, vol. 183, Dec. 2021, Art. no. 108282, doi: 10.1016/j.apacoust.2021.108282.

[19] M. F. Siddique, Z. Ahmad, and J.-M. Kim, "Pipeline leak diagnosis based on leak-augmented scalograms and deep learning," *Eng. Appl. Comput. Fluid Mech.*, vol. 17, no. 1, Dec. 2023, Art. no. 2225577, doi: 10.1080/19942060.2023.2225577.

[20] M. Fahimipirehgalin, E. Trunzer, M. Odenweller, and B. Vogel-Heuser, "Automatic visual leakage detection and localization from pipelines in chemical process plants using machine vision techniques," *Engineering*, vol. 7, no. 6, pp. 758–776, Jun. 2021, doi: 10.1016/j.eng.2020.08.026.

[21] S. Vishnuvardhan, A. R. Murthy, and A. Choudhary, "A review on pipeline failures, defects in pipelines and their assessment and fatigue life prediction methods," *Int. J. Pressure Vessels Piping*, vol. 201, Feb. 2023, Art. no. 104853, doi: 10.1016/j.ijpvp.2022.104853.

[22] M. Abdelghani, G. Tewfik, D. Djahida, and S. S. Ahmed, "Prediction of the rupture pressure of transmission pipelines with corrosion defects," *J. Pressure Vessel Technol., Trans.*, vol. 140, no. 4, Aug. 2018, doi: 10.1115/1.4039698/368028.

[23] B. Glisic and T. Kundu, "Sensing solutions for assessing and monitoring pipeline systems," *Sensor Technol. Civil Infrastruct.*, vol. 2, pp. 255–297, Jan. 2022, doi: 10.1016/B978-0-08-102706-6.00014-3.

[24] A. Smith, I. D. Moore, and N. Dixon, "Acoustic emission sensing of Pipe–Soil interaction: Full-scale pipelines subjected to differential ground movements," *J. Geotechnical Geoenvironmental Eng.*, vol. 145, no. 12, Dec. 2019, Art. no. 04019113.

[25] V. Nasir, S. Ayanleye, S. Kazemirad, F. Sassani, and S. Adamopoulos, "Acoustic emission monitoring of wood materials and timber structures: A critical review," *Construct. Building Mater.*, vol. 350, Oct. 2022, Art. no. 128877, doi: 10.1016/j.conbuildmat.2022.128877.

[26] T.-K. Nguyen, Z. Ahmad, and J.-M. Kim, "A deep-learning-based health indicator constructor using Kullback–Leibler divergence for predicting the remaining useful life of concrete structures," *Sensors*, vol. 22, no. 10, p. 3687, May 2022, doi: 10.3390/s22103687.

[27] T. B. Quy and J.-M. Kim, "Crack detection and localization in a fluid pipeline based on acoustic emission signals," *Mech. Syst. Signal Process.*, vol. 150, Mar. 2021, Art. no. 107254, doi: 10.1016/j.ymssp.2020.107254.

[28] S. Livadiotis, K. Sitaropoulos, A. Ebrahimkhanlou, and S. Salamone, "Acoustic emission monitoring of corrosion in steel pipes using Lamb-type helical waves," *Struct. Health Monit.*, vol. 22, no. 2, pp. 1225–1236, Jun. 2022.

[29] J. Huang, Z. Zhang, R. Qin, Y. Yu, G. Wen, W. Cheng, and X. Chen, "Lightweight neural network architecture for pipeline weld crack leakage monitoring using acoustic emission," *IEEE Trans. Instrum. Meas.*, vol. 72, pp. 1–10, 2023, doi: 10.1109/TIM.2023.3298393.

[30] G. Vachtsevanos, F. L. Lewis, M. Roemer, A. Hess, and B. Wu, *Intelligent Fault Diagnosis and Prognosis for Engineering Systems*. Hoboken, NJ, USA: Wiley, 2006.

[31] C. Ferreira and G. Gonçalves, "Remaining useful life prediction and challenges: A literature review on the use of machine learning methods," *J. Manuf. Syst.*, vol. 63, pp. 550–562, Apr. 2022, doi: 10.1016/j.jmsy.2022.05.010.

[32] C.-H. Hu, H. Pei, X.-S. Si, D.-B. Du, Z.-N. Pang, and X. Wang, "A prognostic model based on DBN and diffusion process for degrading bearing," *IEEE Trans. Ind. Electron.*, vol. 67, no. 10, pp. 8767–8777, Oct. 2020, doi: 10.1109/TIE.2019.2947839.
[33] B. He, L. Liu, and D. Zhang, "Digital twin-driven remaining useful life prediction for gear performance degradation: A review," *J. Comput. Inf. Sci. Eng.*, vol. 21, no. 3, pp. 1–28, Jun. 2021.
[34] G. Prakash, X. X. Yuan, B. Hazra, and D. Mizutani, "Toward a big data-based approach: A review on degradation models for prognosis of critical infrastructure," *J. Nondestruct. Eval. Diagn. Progn. Eng. Syst.*, vol. 4, no. 2, pp. 1–36, May 2021.
[35] N. B. Shaik, S. R. Pedapati, and F. A. B. A. Dzubir, "Remaining useful life prediction of a piping system using artificial neural networks: A case study," *Ain Shams Eng. J.*, vol. 13, no. 2, Mar. 2022, Art. no. 101535, doi: 10.1016/j.asej.2021.06.021.
[36] L. Xu, Y. Wang, L. Mo, Y. Tang, F. Wang, and C. Li, "The research progress and prospect of data mining methods on corrosion prediction of oil and gas pipelines," *Eng. Failure Anal.*, vol. 144, Feb. 2023, Art. no. 106951, doi: 10.1016/j.engfailanal.2022.106951.
[37] E. B. Priyanka, S. Thangavel, X.-Z. Gao, and N. S. Sivakumar, "Digital twin for oil pipeline risk estimation using prognostic and machine learning techniques," *J. Ind. Inf. Integr.*, vol. 26, Mar. 2022, Art. no. 100272, doi: 10.1016/j.jii.2021.100272.
[38] L. Gao and L. Guan, "Interpretability of machine learning: Recent advances and future prospects," *IEEE MultimediaMag.*, vol. 1, no. 1, pp. 1–12, Sep. 2023, doi: 10.1109/MMUL.2023.3272513.
[39] B. Xue, H. Xu, X. Huang, K. Zhu, Z. Xu, and H. Pei, "Similarity-based prediction method for machinery remaining useful life: A review," *Int. J. Adv. Manuf. Technol.*, vol. 121, nos. 3–4, pp. 1501–1531, Jun. 2022, doi: 10.1007/s00170-022-09280-3.
[40] M. Hou, D. Pi, and B. Li, "Similarity-based deep learning approach for remaining useful life prediction," *Measurement*, vol. 159, Jul. 2020, Art. no. 107788, doi: 10.1016/j.measurement.2020.107788.
[41] J. Lyu, R. Ying, N. Lu, and B. Zhang, "Remaining useful life estimation with multiple local similarities," *Eng. Appl. Artif. Intell.*, vol. 95, Oct. 2020, Art. no. 103849, doi: 10.1016/j.engappai.2020.103849.
[42] C. Kong, W. Yu, Q. Zeng, Z. Chen, and Y. Peng, "A similarity-based remaining useful life prediction method using multimodal degradation features and adjusted cosine similarity," *Meas. Sci. Technol.*, vol. 34, no. 10, Jul. 2023, Art. no. 105112, doi: 10.1088/1361-6501/ace20b.
[43] Y. Qin, J. Yang, J. Zhou, H. Pu, and Y. Mao, "A new supervised multi-head self-attention autoencoder for health indicator construction and similarity-based machinery RUL prediction," *Adv. Eng. Informat.*, vol. 56, Apr. 2023, Art. no. 101973, doi: 10.1016/j.aei.2023.101973.
[44] M. A. Richards, *Fundamentals of Radar Signal Processing*, 3rd ed., New York, NY, USA: McGraw-Hill, 2022.
[45] T.-K. Nguyen, Z. Ahmad, and J.-M. Kim, "A scheme with acoustic emission hit removal for the remaining useful life prediction of concrete structures," *Sensors*, vol. 21, no. 22, p. 7761, Nov. 2021, doi: 10.3390/s21227761.
[46] *Non-destructive Testing—Acoustic Emission Testing (AT)—Leak Detection By Means of Acoustic Emission*, Standard ISO 18081:2016, 2016.
[47] A. Saxena, J. Celaya, E. Balaban, K. Goebel, B. Saha, S. Saha, and M. Schwabacher, "Metrics for evaluating performance of prognostic techniques," in *Proc. Int. Conf. Prognostics Health Manage.*, Oct. 2008, pp. 1–20, doi: 10.1109/phm.2008.4711436.
[48] Z. I. Botev, J. F. Grotowski, and D. P. Kroese, "Kernel density estimation via diffusion," *Ann. Statist.*, vol. 799, no. 5, pp. 2916–2957, Oct. 2010.

DUC-THUAN NGUYEN received the B.S. and M.S. degrees in control engineering and automation from the School of Electrical and Electronic Engineering, Hanoi University of Science and Technology (HUST), Vietnam, in 2021 and 2023, respectively. He is currently pursuing the Ph.D. degree in AI and computer engineering with the University of Ulsan, South Korea. His research interests include fault diagnosis and prognostics, advanced signal processing, and AI-enabled systems.

TUAN-KHAI NGUYEN received the B.S. degree from the Faculty of Electronics and Telecommunications, University of Engineering and Technology (UET-VNU), Vietnam National University, Hanoi, Vietnam. He is currently pursuing the Ph.D. degree in computer engineering with the University of Ulsan, South Korea.

After his graduation, he was with the Information and Electronic Warfare Center, VPT, and VIETTEL. He has been a Graduate Research Assistant with Ulsan Industrial Artificial Intelligence (UIAI) Laboratory, University of Ulsan, since 2020. His current research interests include around signal processing, artificial intelligence, fault diagnosis, and prognosis for industrial machinery and structures.

ZAHOOR AHMAD received the B.S. degree in computer engineering from the COMSATS Institute of Information Technology (CIIT), now known as COMSATS University Islamabad (CUI), Attock, Pakistan, in 2016, the M.S. degree in electronics and information engineering from Korea Aerospace University (KAU), Goyang-si, South Korea, in 2019, and the Ph.D. degree from the University of Ulsan, South Korea.

Since 2023, he has been a Postdoctoral Research Fellow with Ulsan Industrial Artificial Intelligence (UIAI) Laboratory, University of Ulsan. His current research interests include artificial intelligence, signal processing, fault diagnosis, condition monitoring of industrial machinery, and fault feature extraction.

JONG-MYON KIM received the B.S. degree in electrical engineering from Myongji University, Yongin-si, South Korea, in 1995, the M.S. degree in electrical and computer engineering from the University of Florida, Gainesville, FL, USA, in 2000, and the Ph.D. degree in electrical and computer engineering from Georgia Institute of Technology, Atlanta, GA, USA, in 2005.

He is currently a Professor with the Department of Electrical, Electronics, and Computer Engineering, University of Ulsan, Ulsan, South Korea. His research interests include fault diagnosis and prognosis, machine learning, multimedia-specific processor architecture, parallel processing, and embedded systems. He is a member of the IEEE Industrial Electronics Society.